Characterization of the response of chromium-doped alumina screens in the vacuum ultraviolet using synchrotron radiation

K. J. McCarthy,[a] A. Baciero, and B. Zurro
Laboratorio Nacional de Fusión, Asociación Euratom-CIEMAT, Avenida Complutense 22, 28040 Madrid, Spain

U. Arp, C. Tarrio, and T. B. Lucatorto
Electron and Optical Physics Division, National Institute of Standards and Technology, Gaithersburg, Maryland 20899

A. Moroño, P. Martín, and E. R. Hodgson
Materiales para Fusión, Laboratorio Nacional de Fusión, Asociación Euratom-CIEMAT, Avenida Complutense 22, 28040 Madrid, Spain

(Received 25 July 2002; accepted 6 September 2002)

We have measured the response of chromium-doped alumina screens to vacuum ultraviolet radiation and derived quantum efficiency curves for the energy range from 30 to 300 eV. A model is presented to explain the structure in this curve. In addition, the radiation hardness of such screens, which have found application as narrow-band radiation detectors for a hot fusion plasma diagnostic, is reported here for MeV electrons. Finally, a simple model is constructed to obtain the carrier diffusion length and the bulk efficiency of this material. © *2002 American Institute of Physics.*
[DOI: 10.1063/1.1518133]

I. INTRODUCTION

Several decades of research on ceramic phosphors at CERN and at other laboratories has led to the almost exclusive use of doped alumina ceramic screens, i.e., $Al_2O_3Cr^{3+}$, for accelerator beam observation.[1] In particular, these screens are compatible with ultrahigh vacuum systems, they exhibit good response linearity, and their radiation resistance is high. For example, in tests made at CERN, screens have withstood integrated relativistic proton fluxes of up to 10^{20} protons cm^{-2}.[1] These levels are a factor $\sim 10^3-10^4$ higher than those for standard phosphors.[2,3] In addition, tests made on polycrystalline Al_2O_3:Cr with He^+ ions accelerated to 200 keV showed a 50% decrease in radioluminescence for total doses above 10^{15} cm^{-2}.[4] This, as well as their immunity to electromagnetic interference and ground loops, as well as their compactness (only a thin screen is required), make them especially suited for use as broadband radiation detectors in the harsh environments encountered in plasma fusion devices.[5]

In previous articles we characterized the response of thin screens of the phosphors $Y_3Al_5O_{12}$:Ce and Y_2O_3:Eu (also known as P-46 and P-22, respectively) using synchrotron radiation between 13.8 and 620 eV and the relative response of Al_2O_3:Cr and other luminescent materials to broadband vacuum ultraviolet (VUV) radiation (15–80 eV) and to hard x rays (5–50 keV).[6,7] The work was motivated by their application as radiation monitors for the TJ-II fusion plasma stellarator device.[8] More recently, a high-spatial resolution detection system incorporating a thin phosphor screen operating in reflection mode has been developed to obtain VUV and soft x-ray radiation profiles of hot plasmas.[9] In the prototype model, tests were made with both P-46 and Al_2O_3:Cr screens. It is now proposed to upgrade this camera by incorporating either multiple thin-foil filter wheels or a multilayer mirror to allow narrow-band radiation to be selected. It is therefore necessary to characterize the spectral response of Al_2O_3:Cr across the VUV and soft x-ray range as it is expected to be nonlinear due to surface and absorption effects, etc.

In this article, we present measurements made using synchrotron radiation on thin Al_2O_3:Cr screens (1-mm thick) over the energy range from 36 to 280 eV (34.2–4.4 nm). From the data, we attempt to identify features present in the excitation spectrum, and we produce curves of the quantum efficiency and intrinsic efficiency of this luminescent material. We also present measurements from a small region of one screen that had been previously irradiated with electrons at integrated fluency of approximately 10^{17} electrons cm^{-2} at 1.8 MeV in order to extend the knowledge on the luminescent radiation limits of this material. Finally, using a simple model we determine the diffusion coefficient length and the light yield for this material.

II. EXPERIMENTAL SETUP

For this work, 46-mm-diameter chrome-doped alumina screens, *Chromox-6*, were obtained from Morgan Matroc Ltd., East Molesey, England.[10] The screens selected are 1-mm thick, they have a density of 3.96 g cm^{-3}, a grain size of 3 to 5 μm, and the alumina was doped with 0.5% chrome sesquioxide. The principal luminescence of Cr^{3+} in Al_2O_3 consists of two sharp lines (generally called the *R* lines), which arise from transitions from the lowest-excited state (^2E) to the $^4A_2$ ground state of Cr^{3+}. At room temperature, these lines occur at 692.9 and 694.3 nm and have a stated

[a]Electronic mail: kieran.mccarthy@ciemat.es

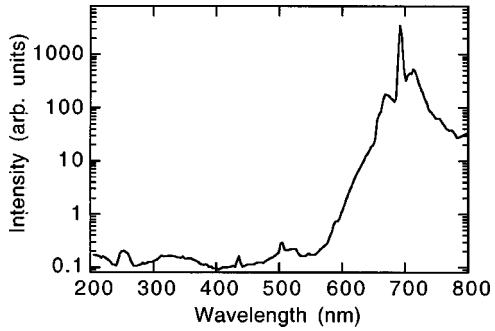

FIG. 1. The emission spectrum of a chrome-doped alumina screen irradiated by 1.8 MeV electrons from the HVEC facility (see Sec. II).

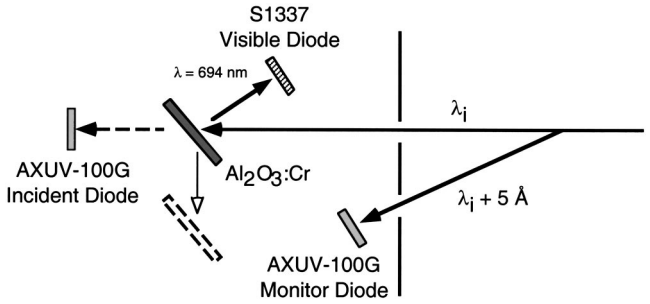

FIG. 2. A schematic diagram of the experimental setup at the NIST/DARPA EUV Reflectometry Facility showing the relative positions of the sample and radiation detectors as well as the incident (λ_i) and emitted light (λ) directions. The screen is displaced to illuminate the incident diode for calibration purposes. A small fraction of the incident beam is diverted to the monitor diode.

decay time of 3.4 ms.[11] Note that this decay time is relatively short compared to the plasma duration in modern fusion devices. Although, additional strong lines may appear with increased Cr^{3+} concentrations, the *R* emission lines dominate for the 0.5% chrome sesquioxide samples and hence are the only emissions considered for analysis. See Fig. 1. In this work, efficiencies are measured in reflection mode only, i.e., the light emerging from the illuminated face of the screen, as the experimental setup did not permit the transmission mode to be studied. However, the efficiency for transmission mode can be approximated empirically as *Chromox-6* screens are translucent, having an attenuation coefficient $\alpha=0.8\pm0.1$ mm^{-1} at the principal fluorescence wavelengths.[1] For this work, two samples were studied, one of which was irradiated as described later.

The efficiency measurements were performed at SURF III on the NIST/DARPA EUV Reflectometry Facility.[12] This is a varied-line-spacing grating monochromator with a 600-mm^{-1} grating working from 35 to 110 eV and a 1500 mm^{-1} grating working from 100 to 300 eV. The resolution varies from 0.02 to 0.07 nm and the throughput is 10^{11} s^{-1} at 95 eV. Thin foil filters (500 nm of C, 500 nm of B, 1000 nm of Be, and 500 nm of Al) provide rejection of multiple grating orders and scattered light. The filter absorption edges also provide wavelength calibration. The incident extreme ultraviolet (EUV) flux is measured using a calibrated EUV-sensitive photodiode, while the emitted visible radiation was measured with a visible-sensitive photodiode. Normalization of the incident radiation was performed by monitoring the throughput of a second exit slit.[13]

Prior to characterization at SURF III, one Al_2O_3:Cr screen was irradiated in a chamber mounted on the beam line of the HVEC 2 MeV Van de Graaff electron accelerator located at CIEMAT.[14] The chamber permits irradiation to be performed under high vacuum ($\leqslant 10^{-6}$ mbar) as well as *in situ* optical emission spectra in the range of 200 to 800 nm to be collected. See Fig. 1. The Al_2O_3:Cr sample was mounted on a water-cooled support set at 45° to the electron beam. It was irradiated for 5 h at 30 °C with 1.8 MeV electrons at a beam current of ~ 0.75 μA cm^{-2}. The resultant ionizing and displacement dose rates were approximately 700 Gy s^{-1} and 10^{-10} displacements per atom per second (dpa s^{-1}), respectively, and the total integrated flux received was $\sim 8.4 \times 10^{16}$ cm^{-2}. The area irradiated was ~ 0.5 cm^2 and when removed from the sample chamber it was identifiable for future testing by a stainlike appearance on its surface.

III. RESULTS AND ANALYSIS

For each beam-line grating, an energy calibration was performed prior to scanning by sequentially placing a set of foil filters in the incident beam and scanning across one or more absorption edges. An AXUV-100G[10] monitor diode was used for this. See Figs. 2 and 3. An energy calibration was made and the offset corrected for by locating the *K*- or *L*-absorption edges in the filters and making a low-order polynomial fit. Once completed, the screen was displaced into the beam and a linear scan across the surface was made at a single energy in order to locate the maximum light output. In general, this was a narrow plateau. Next, the sample was scanned in small energy steps over the entire energy range of the selected grating. At each step, the incident beam energy, the visible diode photocurrent, and the stored beam current were recorded. Once completed, the energy scan was repeated with the sample removed from the beam and the incident diode photocurrent was stored. Also, background measurements were taken with no incident beam present.

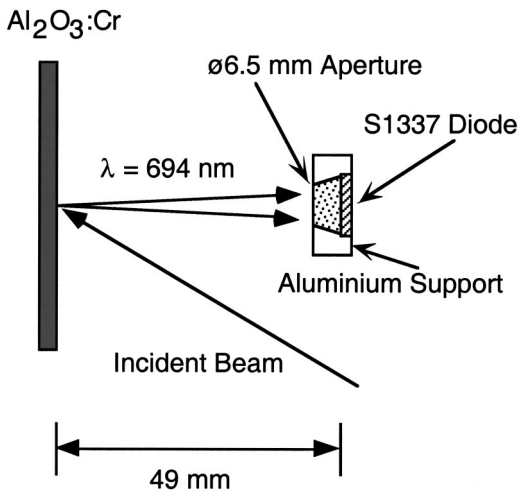

FIG. 3. A schematic diagram showing the alumina screen, the visible diode, and the visible light collection geometry.

Finally, the irradiated region of the first sample was located by performing a linear scan about its predicted position. A drop in output signal over an extended area identified this area.

Several steps were required when postprocessing the data in order to obtain quantum efficiency curves. First, the incident photon flux was estimated from the measured photocurrent at each energy step using the sensitivity curve (A/W) for the EUV-sensitive AXUV-100G photodiode.[15] Second, the luminescence photon flux was determined from the Hamamatsu S1337-1010BR[10] visible diode signals using the quoted photosensitivity (A/W) at the peak emission wavelength.[16] In all cases, the background was $<0.1\%$ of the signal. Then, from the screen/visible diode geometry and by assuming a Lambertian falloff in light intensity as a function of angle to the surface normal, the integrated light flux emitted over 2π steradian from the screen was determined. As the screen to detector separation was relatively small (<50 mm), the beam spot area (~ 20 mm^2 when above ~ 105 eV and ~ 10 mm^2 otherwise) constituted an extended source. Hence, the fractional solid angle to the detector was obtained using equations described in Tsoulfanidis[17] for disk sources which result in a fixed error of $\sim 1\%$ for absolute measurements. The efficiency (number of visible photons emitted from the front surface per incident VUV photon) as a function of wavelength could then be determined. Also, the estimated uncertainty in the measurements is $\pm 17\%$ for the absolute and $\pm 2.5\%$ for relative values. The largest absolute error occurs in the responsivity of the S1337 photodiode, $\pm 15\%$, while the largest contribution to relative error arises from the variations in the measured visible light output ($\pm 1\%$). Finally, splicing together data from overlapping energy ranges created the quantum efficiency curves.

Curves of quantum efficiency for reflection mode are plotted in Fig. 4(a). Here, Al_2O_3:Cr exhibits an almost linear variation with energy. Nonetheless, this curve exhibits significant structures between ~ 78 and 130 eV. See Fig. 4(b). We attribute the sharp drop in efficiency that occurs just above 78 eV, and the features that extend for several tens of electron volts above it, to the aluminum L_3 edge and related extended x-ray absorption fine structures. The edge at 78.4 eV is shifted up by ~ 5.85 eV with respect to the Al L_3 edge in its natural form. This is due to chemical bonding which gives rise to a change of electron configuration in the valence shells, which in turn influences the inner energy levels.[18] Its location is in good agreement with the value of 78.6 eV reported for high-resolution absorption spectra of bulk amorphous Al_2O_3.[19] Furthermore, the features seen above this edge, and their locations, reflect the features seen in the absorption spectra of bulk amorphous Al_2O_3 measured by Brytov and Romashchenko.[20] In particular, the drop in luminescence efficiency above 93 eV, which bottoms out at ~ 99 eV, reflects the increase in absorption coefficient at these energies. See Fig. 5. Also, extending for several electron volts above ~ 105.4 eV, the efficiency curves have a contribution because of a drop in the sensitivity of the AXUV incident photodiode above the chemically shifted L_3 edge of silicon.[15] The effect is seen on the AXUV incident photodiode scan signals but could not be fully removed here. Finally, no drop

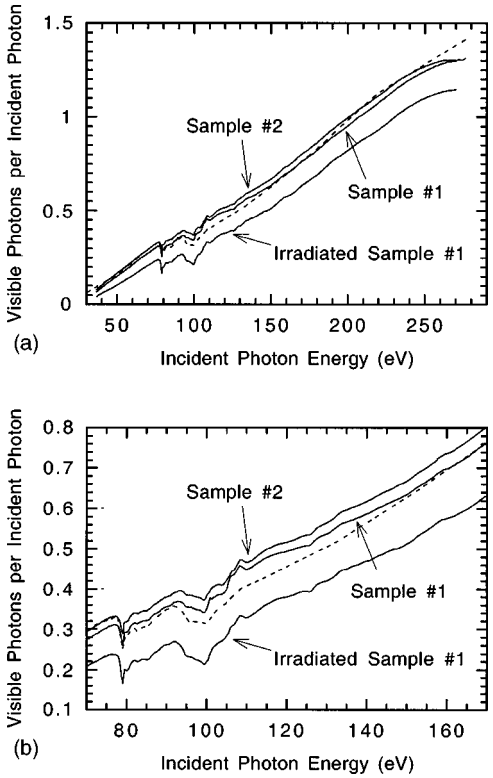

FIG. 4. (a) The quantum efficiency (QE) of the Al_2O_3:Cr screen for the reflection mode of operation. Shown here are the QE curves for two chrome-doped alumina samples, the irradiated section of Sample #1, and the best-fit of the one-dimensional model (broken line). (b) As (a) but for a reduced energy range.

in efficiency is seen above the L_1 edge of oxygen (at 41.6 eV in its natural form) while a small drop in efficiency is seen above 124.5 eV, i.e., the chemically shifted Al L_1 edge (at 117.8 eV in its natural form). This may be expected, as the relative change in absorption across the L_1 edge is significantly less than that across the L_3 edge.

In this section, we apply the simple one-dimensional model developed by Benitez *et al.*,[21] for phosphor screens, with some modifications based on the model developed by Baciero *et al.*,[22] to model our efficiency curves. For this it is assumed that the luminescence intensity is proportional to the number of band electron-hole pairs created, that carrier lifetime is independent of this number, and that carrier mi-

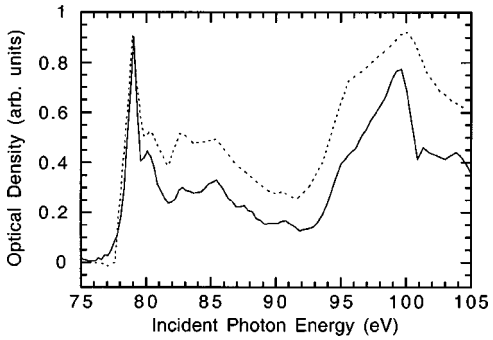

FIG. 5. A comparison of the normalized optical density of amorphous Al_2O_3 by Brytov and Romashchenko (dashed line) with that determined from the luminescence data (continuous line).

gration is a diffusion process with ambipolar diffusion length L. Since the reflection coefficient of amorphous Al_2O_3 is low in this spectral range (<0.1% according to Zhurakovskii *et al.*[23]) we ignore its effects here. The resultant equation for efficiency is

$$QE = \frac{\eta_0 E_i \mu_i'}{E_v}\left(\frac{1}{S}+\frac{1}{1+\mu_i' L}\right)\left(\frac{1}{1+S^{-1}}\right)\int_0^T \exp(-\mu_i' t)\,dt, \quad (1)$$

where η_0 is the energy emitted as photons per incident electron volt, E_i and E_v are incident and visible photon energies, S is the reduced surface recombination velocity, $\mu_i' = \mu_i \cos^{-1}\theta$; where μ_i is attenuation coefficient (m^{-1}), and θ is the angle of incidence of the incident radiation, and t is the depth into the sample of thickness T. Here, the μ_i for Al_2O_3 were determined by interpolating between discrete values estimated from the weighted μ of Al and O of Henke, Gullikson, and Davis,[24] except between 75 and 120 eV, where they were determined from curves in Brytov and Romashchenko.[20] Now, recalling that the curves in Figs. 4 are for reflection mode, we obtain a best fit with η_0, S, and L equal to 0.025, 100 and 155 Å. Note that S cannot be determined very precisely here. The value for L is of the same order as values measured for rare-earth doped phosphors.[21] The resultant equivalent light yield, i.e., 1.4×10^4 photons MeV^{-1}, is very similar to that of the common phosphor P-46 (1.4×10^4 MeV^{-1}).

An overall reduction of 25% in light output is observed from the irradiated part of the ceramic. See Figs. 4(a) and 4(b). This drop varies from ~40% for 35 eV photons to ~10% at the highest energies. For 1.8 MeV electrons, almost all energy loss on passing through a material is by interaction mechanisms that result in ionization of the material. There is minimal momentum transfer to the atoms in the material for creating vacancies or defects, which can compete with emission centers for absorbed energy. For the energy range studied, incident photons are almost completely absorbed within 0.3 μm of the surface, this attenuation length decreasing to tens of nanometers at the lowest energies. Also, while irradiating the screen, no reduction was observed in its radioluminescence output even for the highest dose received. The attenuation length for 1.8 MeV electrons is >2 mm in alumina so radioluminescence is excited along the complete path length through the sample. These findings suggest that the drop in luminescence efficiency from the irradiated ceramic can be attributed to charge losses near grain surfaces. Indeed, one of the principal nonradiative decay channels in phosphors for this energy range is surface recombination. Also, these are long-lived effects as the luminescence measurements were performed several months after irradiation and the sample was kept at room temperature in the intervening period. Now, applying the Birks and Black law for luminescence efficiency loss in irradiated materials,[25]

$$\frac{I}{I_0} = \frac{1}{1+\frac{N}{N_{1/2}}}, \quad (2)$$

where I_0 and I are the output intensities before and after sample irradiation with the total flux N, and $N_{1/2}$ is the flux that reduces the intensity output to half the original. Applying this equation for incident VUV radiation between 30 and 300 eV, the $N_{1/2}$ of Al_2O_3:Cr is $\sim 2.5\times10^{17}$ cm^{-1} for MeV electrons. This is several orders of magnitude lower than that quoted for fast particle applications, i.e., 10^{20} proton cm^{-2}.[1] While some shielding may be required for VUV applications in high-radiation environments, the smaller reduction in the luminescence output at higher-photon energies of Fig. 4(a) suggests that the $N_{1/2}$ of this material for harder x rays will be considerably higher.

IV. CONCLUSIONS

The reflection-mode luminescence efficiency of screens of the chrome-doped alumina *Chromox-6* has been measured for the energy range 36 to 280 eV. A simple model has been fitted to the curves to obtain the intrinsic efficiency of this material, which was found to be similar to that of several commonly used phosphor powders. The material also shows high resistance to radiation damage by MeV electrons, a property that makes it a possible candidate for use in radiation monitors in large-scale fusion devices where high-radiation levels occur.

ACKNOWLEDGMENTS

This work was supported by the Commission for Cultural, Educational and Scientific Exchange between the United States of American and Spain under the Fulbright Program and was partially funded by the Spanish Ministry of Science and Education under Contract DGCYT No. PB97-0160 and Ministry of Science and Technology under Grant No. FTN2000-0922.

[1] C. D. Johnson, *The Development and Use of Alumina Ceramic Fluorescent Screens*, European Laboratory for Particle Physics Report No. CERN/PS/90-42(AR).
[2] M. C. Ross, J. T. Seeman, R. K. Jobe, J. C. Sheppard, and R. F. Stienin, IEEE Trans. Nucl. Sci. **NS-32**, 2003 (1985).
[3] W. A. Hollerman, J. H. Fisher, L. R. Holland, and J. B. Czirr, IEEE Trans. Nucl. Sci. **40**, 1355 (1993).
[4] N. T. My, Y. Aoki, H. Takeshita, S. Yamamoto, P. Goppelt-Langer, and H. Naramoto, in *Proceedings of the 6th Japan-China Bilateral Symposium on Radiation Chemistry*, edited by Y. Hama, Y. Katsumura, N. Kouchi, and K. Makuuchi (Japan Atomic Energy Research Institute, Tokyo, 1995).
[5] B. Zurro, C. Burgos, K. J. McCarthy, and L. Rodriguez Barquero, Rev. Sci. Instrum. **68**, 680 (1997).
[6] A. Baciero, K. J. McCarthy, M. A. Acedo, L. Rodriguez-Barquero, J. Avila, Y. Huttel, V. Perez Dieste, M. C. Asensio, and B. Zurro, J. Synchrotron Radiat. **7**, 215 (2000).
[7] B. Zurro, A. Ibarra, K. J. McCarthy, A. U. Acuña, and R. Sastre, Rev. Sci. Instrum. **66**, 534 (1995).
[8] C. Alejaldre, J. Alonso, L. Almoguera, E. Ascasíbar, A. Baciero, R. Balbín, M. Blaumoser, J. Botija, B. Brañas, E. de la Cal, A. Cappa, R. Carrasco, F. Castejón, J. R. Cepero, C. Cremy, J. Doncel, C. Dulya, T. Estrada, A. Fernández, M. Francés, C. Fuentes, A. García, I. García-Cortes, J. Guasp, J. Herranz, C. Hidalgo, J. A. Jiménez, I. Kirpitchev, V. Krivenski, I. Labrador, F. Lapayse, K. Likin, M. Liniers, A. López-Fraguas, A. López-Sánchez, E. de la Luna, R. Martín, A. Martínez, M. Medrano, P. Méndez, K. J. McCarthy, P. Medina, B. van Milligen, M. Ochando, L. Pacios, I. Pastor, M. A. Pedrosa, A. de la Peña, A. Portas, J. Qin, L. Rodríguez-Rodrigo, A. Salas, E. Sánchez, J. Sánchez, F. Tabarés, D. Tafalla, V. Tribaldos, J. Vega, B. Zurro, D. Akulina, O. I. Fedyanin, S. Grebenshchicov, N. Kharchev, A. Meshcheryakov, R. Barth, G. van Dijk, H. van der

Meiden, and S. Petrov, Plasma Phys. Controlled Fusion **41**, A539 (1999).
[9] A. Baciero, B. Zurro, K. J. McCarthy, P. Martin, and M. C. de la Fuente, Rev. Sci. Instrum. **73**, 283 (2002).
[10] Certain commercial equipment, instruments, or material are identified in this article to foster understanding. Such identification does not imply recommendation or endorsement by the National Institute of Standards and Technology, nor dies it imply that the materials or equipment identified are necessarily the best available for the purpose.
[11] M. Tamatani, in *Phosphor Handbook*, edited by S. Shionoya and W. M. Yen, (CRC Press, Boca Raton, 1998).
[12] C. Tarrio, R. N. Watts, T. B. Lucatorto, M. Haass, T. A. Calcott, and J. Jia, J. X-Ray Sci. Technol. **4**, 96 (1994).
[13] C. Tarrio, T. B. Lucatorto, S. Grantham, M. B. Squires, U. Arp, and L. Deng, in *Proceedings of Soft X-ray and EUV Imaging Systems II*, Vol. 4506, edited by D. A. Tichenor and J. A. Folta (SPIE Conference Proceedings, 32, 2001).
[14] A. Moroño and E. R. Hodgson, J. Nucl. Mater. **224**, 216 (1995).
[15] E. M. Gullikson, R. Korde, L. R. Canfield and R. E. Vest, J. Electron Spectrosc. Relat. Phenom. **80**, 313 (1996).
[16] Si Photodiode S1337 Series Technical Data Sheet, Hamamatsu Photonics K.K., Solid State Division, Hamamatsu City, Japan (2001).
[17] N. Tsoulfanidis, *Measurement and Detection of Radiation*, McGraw-Hill series in Nuclear Engineering, (Hemisphere Publishing Corporation, Washington, 1983).
[18] B. K. Agarwal, *X-ray Spectroscopy: An Introduction*, Springer Series in Optical Sciences, Springer-Verlag New York, 1991).
[19] A. Balzarotti, F. Antonangeli, R. Girlanda, and G. Martino, Phys. Rev. B **29**, 5903 (1984).
[20] I. A. Brytov and Y. N. Romashchenko, Fiz. Tverd. Tela (Leningrad) **20**, 664 (1978) [Sov. Phys. Solid State **20**, 384 (1978)].
[21] E. L. Benitez, D. E. Husk, S. E. Schnatterly, and C. Tarrio, J. Appl. Phys. **70**, 3256 (1991).
[22] A. Baciero, L. Placentino, K. J. McCarthy, L. R. Barquero, A. Ibarra, and B. Zurro, J. Appl. Phys. **85**, 6790 (1999).
[23] A. P. Zhurakovskii, E. S. Gluskin, and M. A. Élango, Fiz. Tverd. Tela (Leningrad) **21**, 233 (1979) [Sov. Phys. Solid State **21**, 138 (1979)].
[24] B. L. Henke, E. M. Gullikson, and J. C. Davis, At. Data Nucl. Data Tables **54**, 181 (1993).
[25] J. B. Birks and F. A. Black, Proc. Phys. Soc. London **64**, 511 (1951).